

This document is the author's final manuscript of

T.L. Huang, M.N. Ichchou, O. Bareille, M. Collet & M. Ouisse: Traveling wave control in thin-walled structures through shunted piezoelectric patches. *Mechanical Systems and Signal Processing*, 2013.

This paper has been published by Elsevier and can be found at <http://dx.doi.org/10.1016/j.ymssp.2012.06.014>

Traveling wave control in thin-walled structures through shunted piezoelectric patches

T.L. Huang^a, M.N. Ichchou^{a,*}, O.A. Bareille^a, M. Collet^b, M. Ouisse^b

^a*LTDS UMR5513 Ecole Centrale de Lyon, 36 Avenue Guy de Collongue, 69134 Ecully, France*

^b*FEMTO-ST, Department of Applied Mechanics, UMR-CNRS 6174, 24 Chemin de l'Épitaphe, 25000 Besançon, France*

Abstract

The wave propagation problem in thin-walled elastic structures with shunted piezoelectric patches is investigated in this work. Based on the finite element(FE) method and periodical structure theory, the Wave Finite Element(WFE) approach is firstly developed as a prediction tool for wave propagation characteristics in thin-walled beam structures, and subsequently extended to consider shunted piezoelectric elements through the Diffusion Matrix Model(DMM). These numerical techniques enable the calculation of reflection and transmission coefficients of propagating waves in thin-walled structures with shunted piezoelectric patches. The performance of shunted piezoelectric patches on the control of wave propagation is analyzed numerically with the DMM. Forced response of thin-walled structures with shunted piezoelectric patches can also be obtained via the Forced Wave Finite Element(FWFE) formulation. With the frequency response issued from the FWFE calculation, the time response of these structures can be acquired

*Corresponding author. Tel.:(33)4 72 18 62 30; fax: (33)4 72 18 91 44.
Email address: mohamed.ichchou@ec-lyon.fr (M.N. Ichchou)

via an Inverse Discrete Fourier Transform(IDFT) approach. An extraction technique for reflection coefficient is proposed and can be applied in both numerical simulations and experiments. The formulations proposed in this work are general and can be applied to all types of slender structures.

Keywords:

Semi-active control, wave propagation, thin-walled structure, piezoelectric, energy diffusion

1. Introduction

Thin-walled structures are widely used nowadays, especially in aerospace engineering domain, where we should solve materials-consumption problems with preservation of necessary strength and sufficient lightness. The aeronautical structures are often large and complex, where the propagation phenomena play an important role in the dynamical behavior of these structures. The thin-walled components, especially straight ones of constant cross-section that can be regarded as one-dimensional waveguides, are often carriers of mechanical energy from the source. The energy transfer leads to sound radiation and unwanted vibration, and then problems like fatigue and structural borne sound will appear. Mastering the dynamical behavior of thin-walled structures can provide efficient and satisfactory means for the structure design.

For this purpose, firstly, prediction and evaluation tools should be developed for thin-walled structures. As waveguides, their dynamic properties can be described by dispersion curves, for which many approaches are available. The most well-known methods are based on theories like Euler-Bernoulli and

Timoshenko beams. However, these beam theories are limited by the hypothesis of undeformed cross-section, which is only valid at low frequencies and for compact cross-sections. In the work of Gavric [1], it is mentioned that when thin-walled beams are concerned, even a relatively low-frequency excitation can produce transfer of mechanical energy by propagating waves associated with deformed cross-section modes. The application of finite element method(FEM) somehow solved this kind of problem, and can give precise prediction of propagational wavenumbers and modes of thin-walled beams. Gavric [1, 2] proposed a particular finite element scheme allowing the extraction of wavenumbers from the resolution of a four-order matrix equation. Gendy *et al.* [3] presented a three-dimensional, two-field variational formulation and the corresponding finite element discretization for free vibration analysis of coupled extensional/flexural/torsional modes of curved beams with arbitrary thin-walled sections. Mitra *et al.* [4] developed a composite thin wall beam element of arbitrary cross-section with open or closed contour. Later, Houillon *et al.* [5] provided a propagative approach in order to extract propagation parameters and the dispersion curves of thin-walled structures of any cross-section. The formulations applied in this work can be referred as wave finite element(WFE) method [6, 7, 8, 9, 10, 11], which has been initiated by Mead [12] and Zhong and Williams [13] for wave mode description into elastic systems with complex cross-sections. This method is not constrained by low-frequency analytical assumptions and can be applied in the mid-frequency range, where cross-section modes propagate [6, 14]. In order to control wave modes propagating in thin-walled structures, appropriate control techniques should be applied, among which the piezoelectric

damping is well adapted. The material's intrinsic passive mechanical behavior can be controlled through piezoelectric transducers in order to attain new desired functionalities [15]. Among the control configurations found in published works, a well-known technique is the piezoelectric damping using external resistor-inductor shunt circuit [15, 16, 17, 18, 19, 20, 21]. This semi-active configuration has the advantage of guaranteeing stability, and can be obtained by bonding piezoelectric elements onto a structure and connecting the electrodes to the external shunt circuit. Due to straining of the host structure, and through the direct piezoelectric effect, a portion of the mechanical energy is converted into electrical energy and subsequently be dissipated by Joule heating via the connected resistor. The $R - L$ shunt circuit on piezoelectric patches can be regarded as light oscillators instead of heavy mass-spring structures. By varying the inductance L in the shunt circuit, the tuning frequency can be adjusted to desired frequency band.

To analyze the propagation of wave modes in thin-walled structures with piezoelectric elements, besides techniques for the prediction of dynamical behavior of waveguides like the WFE method, piezoelectric finite elements should also be integrated in the numerical model so as to consider the piezoelectric domain in the structure. Recently, structures with shunted piezoelectric elements were treated properly with FEM in the work of Nguyen and Pietrzko [18] and Becker *et al.* [19]. However, the excessive computational time associated with large models constitutes one of the major limitations. As an alternative, the WFE formulation with piezoelectric elements can provide a low cost and efficient way to capture the dynamic behavior of those structures. Spadoni *et al.* [20] and Casadei *et al.* [21] have studied

the control of wave propagation in plates with periodic arrays of shunted piezoelectric patches. Efforts have been dedicated firstly to developing the finite element formulation of shunted piezoelectric elements, then to characterizing the dispersion relation of waves propagating over the surface of plate structures and the band gaps in the frequency domain. An experimental investigation was carried out in the work of Casadei *et al.* [21] to test the performance of shunted piezoelectric patches via the forced response of the structure. Wang *et al.* [22] have realized the same analysis on a beam with periodic shunted piezoelectric patches through an analytical model and corresponding experimental tests. Collet *et al.* [15] provided a full finite element description of a beam with periodic shunted piezoelectric patches via the WFE method, but emphasis was placed on the optimization of shunt impedance. Appropriate numerical tools still need to be properly developed so as to characterize wave propagation and energy diffusion properties for thin-walled structures with shunted piezoelectric elements.

Efforts have been made in this work to provide general formulations for thin-walled structures with shunted piezoelectric patches. It should be mentioned that these formulations can be applied for all kinds of elastic slender structures. On the whole, this paper focuses on proposing efficient numerical tools for the prediction of wave propagation characteristics and dynamic behavior of thin-walled beam structures with shunted piezoelectric patches. Verification procedures are also considered in this work to test the efficiency of all the numerical techniques for the evaluation of wave propagation characteristics and dynamic behavior of those structures. This paper is organized as follows: in Section 2, a brief outline of the WFE approach is provided (Sub-

section 2.1). Subsequently, the numerical approach to evaluate the forced response of the structure, namely the Forced Wave Finite Element(FWFE) approach, is described (Subsection 2.2). The technique to acquire time response of the structure is introduced in Subsection 2.3. Thereafter, the DMM formulation for the prediction of energy diffusion of wave modes propagating in thin-walled beam with shunted piezoelectric patches is presented (Subsection 2.4). All these numerical techniques are applied in Section 3 to evaluate the performance of the shunted piezoelectric patches on the control of wave modes in the beam. The symmetric pumping wave mode and the extensional wave mode are targeted and investigated numerically via the DMM in Subsection 3.1, and then through the FWFE approach in Subsection 3.2. In Subsection 3.3, the thin-walled beam is excited in the extensional mode with a wave packet excitation, and corresponding frequency and time responses are calculated, based on which the reflection coefficients can be extracted to verify DMM simulation results. Concluding remarks and perspectives of this work are presented in Section 4.

2. Numerical prediction tools for thin-walled structures with shunted piezoelectric elements

In this section, firstly the WFE formulation and the DMM are presented. Then the forced WFE formulation and the method for the extraction of time response are presented. All these techniques enable the calculation of parameters like reflection and transmission coefficients, the frequency response function(FRF), and the time response under wave packet excitation. At last, the finite element model of thin-walled beam structure with shunted piezo-

electric elements is described in detail. With this model, the DMM can be extended to consider piezoelectric elements so as to investigate the influence of the shunted piezoelectric patches on the propagation of wave modes in thin-walled beams. The formulations developed are general and can be employed for all types of elastic slender structures with shunted piezoelectric patches.

2.1. Wave propagation and diffusion in structures through finite elements

The WFE method was employed to study the energy diffusion problem [6, 9, 23]. These references provide a detailed description of the dynamical behavior of a slender structure, as illustrated in Figure 1, which is composed, along a specific direction (say X -axis), of N identical substructures. Note that this general description can be applied to homogeneous systems whose cross-sections are constant. The dynamic of the global system is formulated from the description of the waves propagating along the X -axis.

Figure 1

Let us consider a finite element model of a given substructure k ($k \in \{1, \dots, N\}$) belonging to the waveguide (cf. Figure 1). The left and right boundaries of the discretized substructure are assumed to contain n degrees of freedom (DOFs). Displacements \mathbf{q} and forces \mathbf{F} which are applied on these boundaries are denoted by $(\mathbf{q}_L, \mathbf{q}_R)$ and $(\mathbf{F}_L, \mathbf{F}_R)$, respectively. It is assumed that the kinematic quantities are represented through state vectors $\mathbf{u}_L^{(k)} = ((\mathbf{q}_L^{(k)})^T (-\mathbf{F}_L^{(k)})^T)^T$ and $\mathbf{u}_R^{(k)} = ((\mathbf{q}_R^{(k)})^T (\mathbf{F}_R^{(k)})^T)^T$, and that the internal DOFs of substructure k are not submitted to external forces.

The dynamical equilibrium of any substructure k can be formulated in this

manner:

$$\mathbf{D} \begin{pmatrix} \mathbf{q}_L^{(k)} \\ \mathbf{q}_I^{(k)} \\ \mathbf{q}_R^{(k)} \end{pmatrix} = \begin{pmatrix} \mathbf{F}_L^{(k)} \\ \mathbf{0} \\ \mathbf{F}_R^{(k)} \end{pmatrix}, \quad (1)$$

where \mathbf{q}_I represents the displacements of the internal dof's of the substructure and \mathbf{D} is a symmetric matrix $\mathbf{D}^T = \mathbf{D}$, representing the complex dynamical stiffness of the substructure:

$$\mathbf{D} = -\omega^2 \mathbf{M} + \mathbf{K}(1 + i\eta). \quad (2)$$

According to Mencik and Ichchou [6], the continuity conditions between the substructures combined with the periodicity condition and the dynamical equilibrium of each substructure can finally lead to the following boundary value problem:

$$\mathbf{S}\Phi_i = \mu_i \Phi_i \quad , \quad |\mathbf{S} - \mu_i \mathbf{I}_{2n}| = 0. \quad (3)$$

where

$$\mathbf{S} = \left[\begin{array}{c|c} -(\mathbf{D}_{LR}^*)^{-1} \mathbf{D}_{LL}^* & -(\mathbf{D}_{LR}^*)^{-1} \\ \hline \mathbf{D}_{RL}^* - \mathbf{D}_{RR}^* (\mathbf{D}_{LR}^*)^{-1} \mathbf{D}_{LL}^* & -\mathbf{D}_{RR}^* (\mathbf{D}_{LR}^*)^{-1} \end{array} \right]. \quad (4)$$

\mathbf{D}^* stands for the dynamical stiffness matrix of substructure k , condensed on the DOFs of the left and right boundaries of the substructure:

$$\mathbf{D}^* = \begin{bmatrix} \mathbf{D}_{LL}^* & \mathbf{D}_{LR}^* \\ \mathbf{D}_{RL}^* & \mathbf{D}_{RR}^* \end{bmatrix}. \quad (5)$$

The matrix \mathbf{I}_{2n} is defined in the following manner:

$$\mathbf{I}_{2n} = \begin{bmatrix} \mathbf{I}_n & \mathbf{0} \\ \mathbf{0} & \mathbf{I}_n \end{bmatrix} \quad (6)$$

where \mathbf{I}_n represents the identity matrix of size n .

As mentioned in reference [15], the eigenvalues μ_i and wavenumbers k_i are linked through the relation $\mu_i = e^{-ik_id_x}$, where d_x denotes the length of the unit cell in X -axis. The sign of the real part of the wavenumber $k_i, Re(k_i)$, represents the direction of the phase velocity of the corresponding waves: if $Re(k_i) > 0$, the phase propagates in the positive x direction; if $Re(k_i) < 0$, the phase propagates in the negative direction, and if it is zero, k_i corresponds to the wavenumber of a pure evanescent wave that only occurs when an undamped system is considered [24]. The matrix Φ of the eigenvectors can be described in this way:

$$\Phi = \begin{bmatrix} \Phi_{\mathbf{q}}^{\text{inc}} & \Phi_{\mathbf{q}}^{\text{ref}} \\ \Phi_{\mathbf{F}}^{\text{inc}} & \Phi_{\mathbf{F}}^{\text{ref}} \end{bmatrix}, \quad (7)$$

where subscripts \mathbf{q} and \mathbf{F} refer to the components which are related to the displacements and the forces, respectively; $((\Phi_{\mathbf{q}}^{\text{inc}})^T(\Phi_{\mathbf{F}}^{\text{inc}})^T)^T$ and $((\Phi_{\mathbf{q}}^{\text{ref}})^T(\Phi_{\mathbf{F}}^{\text{ref}})^T)^T$ stand for the modes which are incident to and reflected by a specific boundary (left or right) of the heterogeneous waveguide, respectively. Finally, assuming modal decomposition, state vectors $\mathbf{u}_{\mathbf{L}}^{(k)}$ and $\mathbf{u}_{\mathbf{R}}^{(k)}$ of any substructures k can be expressed from eigenvectors $\{\Phi_i\}_{i=1,\dots,2n}$ [13]:

$$\mathbf{u}_{\mathbf{L}}^{(k)} = \Phi \mathbf{Q}^{(k)}, \quad \mathbf{u}_{\mathbf{R}}^{(k)} = \Phi \mathbf{Q}^{(k+1)} \quad \forall k \in \{1, \dots, N\}. \quad (8)$$

Here, vector \mathbf{Q} stands for the amplitudes of the wave modes, which can be expressed by (cf. equation(7)):

$$\mathbf{Q} = \begin{pmatrix} \mathbf{Q}^{\text{inc}} \\ \mathbf{Q}^{\text{ref}} \end{pmatrix}. \quad (9)$$

The dynamical behavior of a periodic waveguide can be simply expressed from a basis of modes representing waves traveling in the positive and negative directions of the system. An analysis of the dynamical response consists of evaluating a set of amplitudes $\{(\mathbf{Q}^{\text{inc}(k)}, \mathbf{Q}^{\text{ref}(k)})\}_k$ associated with the incident and reflected modes. Nevertheless, to evaluate energy diffusion, the formulation of the coupling conditions of the system is needed, and particularly at a coupling junction where several waveguides can be considered. It should be mentioned that the whole system has free boundary conditions, and the coupling conditions are in fact boundary conditions for subsystems (waveguides and coupling element).

Figure 2

Let us consider two periodic waveguides which are coupled through a coupling element and let us consider two corresponding substructures (1 and 2) which are located at the ends of the waveguides (see Figure 2). These substructures are coupled with the coupling element at surfaces Γ_1 and Γ_2 and are coupled with the other substructures, into waveguides, at surfaces S_1 and S_2 . It is assumed that the coupling element is only subject to the coupling actions (i.e. there is no force inside the element).

According to Mencik and Ichchou [6], with the dynamical equilibrium of the wave guides and the coupling element, and their continuity conditions of nodal displacement and force expressed in the modal basis, it can be demonstrated that the dynamical behavior of a given coupled periodic waveguide i ($i = 1, 2$) can be simply expressed in terms of wave modes $((\Phi_{\mathbf{q}}^{\text{inc}(i)})^T (\Phi_{\mathbf{F}}^{\text{inc}(i)})^T)^T$ incident to the coupling element and wave modes $((\Phi_{\mathbf{q}}^{\text{ref}(i)})^T (\Phi_{\mathbf{F}}^{\text{ref}(i)})^T)^T$ reflected by the coupling element.

The dynamical equilibrium of a discretized substructure i ($i = 1, 2$) and the coupling element can be formulated in this way:

$$\mathbf{D}^{(i)} \begin{pmatrix} \mathbf{q}_L^{(i)} \\ \mathbf{q}_I^{(i)} \\ \mathbf{q}_R^{(i)} \end{pmatrix} = \begin{pmatrix} \mathbf{F}_L^{(i)} \\ \mathbf{0} \\ \mathbf{F}_R^{(i)} \end{pmatrix} \quad (i = 1, 2) \quad \text{and} \quad \mathbb{K} \begin{pmatrix} \mathbf{q}_1^c \\ \mathbf{q}_I^c \\ \mathbf{q}_2^c \end{pmatrix} = \begin{pmatrix} \mathbf{F}_1^c \\ \mathbf{0} \\ \mathbf{F}_2^c \end{pmatrix}, \quad (10)$$

where matrix \mathbb{K} stands for the complex dynamical stiffness of the coupling element, $(\mathbf{q}_1^c, \mathbf{F}_1^c)$ and $(\mathbf{q}_2^c, \mathbf{F}_2^c)$ represent the displacements and the forces applied at the dof's of the coupling element on surfaces Γ_1 and Γ_2 , respectively. Assuming that on surfaces Γ_1 and Γ_2 , the coupling element and the waveguides have the same meshing, so the continuity conditions between them can be simply expressed as:

$$\begin{bmatrix} \mathbf{q}_1^c \\ \mathbf{q}_2^c \end{bmatrix} = \begin{bmatrix} \mathbf{q}_R^{(1)} \\ \mathbf{q}_L^{(2)} \end{bmatrix}, \quad \begin{bmatrix} \mathbf{F}_1^c \\ \mathbf{F}_2^c \end{bmatrix} = - \begin{bmatrix} \mathbf{F}_R^{(1)} \\ \mathbf{F}_L^{(2)} \end{bmatrix} \quad (11)$$

The dynamical equilibrium of the coupling element can be expressed in a condensed form

$$\mathbb{K}^* \begin{pmatrix} \mathbf{q}_1^c \\ \mathbf{q}_2^c \end{pmatrix} = \begin{pmatrix} \mathbf{F}_1^c \\ \mathbf{F}_2^c \end{pmatrix}, \quad (12)$$

where \mathbb{K}^* stands for the dynamical stiffness matrix of the coupling element, condensed on the DOFs located on surfaces Γ_1 and Γ_2 .

The relation between forces $(\mathbf{F}_R^{(1)}, \mathbf{F}_L^{(2)})$ applied at the right and left boundaries of substructures 1 and 2 and displacements $(\mathbf{q}_R^{(1)}, \mathbf{q}_L^{(2)})$ is easily found by considering equations (12) and (11):

$$\mathbb{K}^* \begin{pmatrix} \mathbf{q}_R^{(1)} \\ \mathbf{q}_L^{(2)} \end{pmatrix} = - \begin{pmatrix} \mathbf{F}_R^{(1)} \\ \mathbf{F}_L^{(2)} \end{pmatrix}. \quad (13)$$

By expressing \mathbf{q} and \mathbf{F} via Equations (8) and (9), the following relation can be obtained:

$$\mathbb{K}^* \begin{pmatrix} \Phi_{\mathbf{q}}^{\text{inc}(1)} \mathbf{Q}^{\text{inc}(1)} + \Phi_{\mathbf{q}}^{\text{ref}(1)} \mathbf{Q}^{\text{ref}(1)} \\ \Phi_{\mathbf{q}}^{\text{inc}(2)} \mathbf{Q}^{\text{inc}(2)} + \Phi_{\mathbf{q}}^{\text{ref}(2)} \mathbf{Q}^{\text{ref}(1)} \end{pmatrix} = - \begin{pmatrix} \Phi_{\mathbf{F}}^{\text{inc}(1)} \mathbf{Q}^{\text{inc}(1)} + \Phi_{\mathbf{F}}^{\text{ref}(1)} \mathbf{Q}^{\text{ref}(1)} \\ \Phi_{\mathbf{F}}^{\text{inc}(2)} \mathbf{Q}^{\text{inc}(2)} + \Phi_{\mathbf{F}}^{\text{ref}(2)} \mathbf{Q}^{\text{ref}(1)} \end{pmatrix}. \quad (14)$$

By rearranging Equation (14), it can be proved that amplitudes $(\mathbf{Q}^{\text{ref}(1)}, \mathbf{Q}^{\text{ref}(2)})$ of the modes reflected by the coupling element can be related to amplitudes $(\mathbf{Q}^{\text{inc}(1)}, \mathbf{Q}^{\text{inc}(2)})$ of the modes incident to the coupling element via a diffusion matrix, namely \mathbb{C} , which relates the reflection and transmission coefficients of the wave modes through the dynamical behavior of the coupling element:

$$\begin{pmatrix} \mathbf{Q}^{\text{ref}(1)} \\ \mathbf{Q}^{\text{ref}(2)} \end{pmatrix} = \mathbb{C} \begin{pmatrix} \mathbf{Q}^{\text{inc}(1)} \\ \mathbf{Q}^{\text{inc}(2)} \end{pmatrix}, \quad (15)$$

with

$$\mathbb{C} = - \left(\mathbb{K}^* \begin{bmatrix} \Phi_{\mathbf{q}}^{\text{ref}(1)} & \mathbf{0} \\ \mathbf{0} & \Phi_{\mathbf{q}}^{\text{ref}(2)} \end{bmatrix} + \begin{bmatrix} \Phi_{\mathbf{F}}^{\text{ref}(1)} & \mathbf{0} \\ \mathbf{0} & \Phi_{\mathbf{F}}^{\text{ref}(2)} \end{bmatrix} \right)^{-1} \times \left(\mathbb{K}^* \begin{bmatrix} \Phi_{\mathbf{q}}^{\text{inc}(1)} & \mathbf{0} \\ \mathbf{0} & \Phi_{\mathbf{q}}^{\text{inc}(2)} \end{bmatrix} + \begin{bmatrix} \Phi_{\mathbf{F}}^{\text{inc}(1)} & \mathbf{0} \\ \mathbf{0} & \Phi_{\mathbf{F}}^{\text{inc}(2)} \end{bmatrix} \right) \quad (16)$$

The diffusion matrix \mathbb{C} directly depends on the normalization of eigenvectors $\{\Phi_j^{(1)}\}_j$ and $\{\Phi_k^{(2)}\}_k$. It seems advantageous to normalize the eigenvectors of the two waveguides in a similar manner. When there is only one unit incident wave mode from waveguide 1, and assuming that there is no incident wave from waveguide 2, we have $\mathbf{Q}^{\text{inc}(1)} = \{0 \ 0 \ \dots \ 0 \ 1 \ 0 \ \dots \ 0\}^T$ and $\mathbf{Q}^{\text{inc}(2)} = \{\mathbf{0}\}$, and the reflection and transmission coefficients \mathbf{C}^{ref} and $\mathbf{C}^{\text{trans}}$ of a

specific incident mode i can be calculated in the following manner:

$$\mathbf{C}_i^{\text{ref}} = \mathbf{Q}_i^{\text{ref}(1)} \quad (17)$$

$$\mathbf{C}_i^{\text{trans}} = \mathbf{Q}_i^{\text{ref}(2)} \quad (18)$$

It should also be mentioned that the matrices \mathbf{S} , \mathbf{D}^* , \mathbb{K}^* and \mathbb{C} are dependent on the frequency.

2.2. Forced Wave Finite Element formulation

The WFE formulation provides wave propagation predictions under free boundary conditions. In order to obtain the forced response of the structure, the Forced Wave Finite Element(FWFE) formulation [7, 25, 26] can be employed. As mentioned in section 2.1, based on equation (8) and equation (9), amplitudes $\mathbf{Q}^{(k)}$ which reflect for instance the kinematic variable $\mathbf{u}_L^{(k)}$ for substructure k , are described from amplitudes $\mathbf{Q}^{(1)}$ and $\mathbf{Q}^{(N+1)}$ representing kinematic variables $\mathbf{u}_L^{(1)}$ and $\mathbf{u}_R^{(N)}$ at the waveguide boundaries. According to the coupling relations between two consecutive substructures k and $k - 1$ ($k \in \{2, \dots, N\}$), $\mathbf{q}_L^{(k)} = \mathbf{q}_R^{(k-1)}$ and $-\mathbf{F}_L^{(k)} = \mathbf{F}_R^{(k-1)}$, the following relation can be found:

$$\mathbf{u}_L^{(k)} = \mathbf{u}_R^{(k-1)} \quad \forall k \in \{2, \dots, N\} \quad (19)$$

which leads to

$$\mathbf{u}_L^{(k)} = \mathbf{S}\mathbf{u}_L^{(k-1)} \quad \forall k \in \{2, \dots, N\} \quad (20)$$

equation (20) allows to write:

$$\mathbf{u}_L^{(k)} = \mathbf{S}^{k-1}\mathbf{u}_L^{(1)} \quad \forall k \in \{1, \dots, N\} \quad (21)$$

with $\mathbf{S}^0 = \mathbf{I}_{2n}$, and:

$$\mathbf{u}_R^{(N)} = \mathbf{S}^N \mathbf{u}_L^{(1)} \quad (22)$$

equation (21) and equation (22) are projected on the basis $\{\Phi_i\}_i$ considering equation (8). Since matrix Φ is invertible (it has been assumed that $\det[\Phi] \neq 0$), one obtains [27]:

$$\mathbf{Q}^{(k)} = \Phi^{-1} \mathbf{S}^{k-1} \Phi \mathbf{Q}^{(1)} \quad \forall k \in \{1, \dots, N+1\} \quad (23)$$

that is (cf. equation (3))

$$\mathbf{Q}^{(k)} = \begin{bmatrix} \Lambda & \mathbf{0} \\ \mathbf{0} & \Lambda^{-1} \end{bmatrix}^{k-1} \mathbf{Q}^{(1)} \quad \forall k \in \{1, \dots, N+1\} \quad (24)$$

where Λ stands for the $(n \times n)$ diagonal eigenvalue matrix for wave modes propagating in x positive direction, expressed by equation (25) [27].

$$\Lambda = \begin{bmatrix} \mu_1 & 0 & \dots & 0 \\ 0 & \mu_2 & \dots & 0 \\ \vdots & \vdots & \ddots & \vdots \\ 0 & 0 & \dots & \mu_n \end{bmatrix} \quad (25)$$

Expressing the boundary conditions of the waveguides in terms of amplitudes $\mathbf{Q}^{(1)}$ and $\mathbf{Q}^{(N+1)}$ allows us to express, from equation (24), the dynamics of a given substructure k . In a general manner, the boundary conditions at a specific boundary of the waveguide can be formulated in this way:

$$\mathbf{Q}^{\text{ref}}|_{\text{lim}} = \mathbb{C} \mathbf{Q}^{\text{inc}}|_{\text{lim}} + \mathcal{F} \quad (26)$$

where \mathbb{C} is the diffusion matrix, and \mathcal{F} stands for the effects of the excitations sources [7, 28]. It is demonstrated in the work of Mencik *et al.* [7] that the

general relation in equation (26) can be applied to describe classical Neumann and Dirichlet boundary conditions. These conditions can be expressed as follows:

$$[\mathbf{0} \mid \mathbf{I}] \mathbf{u} = \mathbf{F}_0 \quad (\text{Neumann}) \quad (27a)$$

$$[\mathbf{I} \mid \mathbf{0}] \mathbf{u} = \mathbf{q}_0 \quad (\text{Dirichlet}) \quad (27b)$$

They can be rewritten in the following manner via the projection of the state vector \mathbf{u} onto the wave mode basis(see equation (8)):

$$\Phi_{\mathbf{F}}^{\text{inc}} \mathbf{Q}^{\text{inc}} + \Phi_{\mathbf{F}}^{\text{ref}} \mathbf{Q}^{\text{ref}} = \mathbf{F}_0 \quad (\text{Neumann}) \quad (28a)$$

$$\Phi_{\mathbf{q}}^{\text{inc}} \mathbf{Q}^{\text{inc}} + \Phi_{\mathbf{q}}^{\text{ref}} \mathbf{Q}^{\text{ref}} = \mathbf{q}_0 \quad (\text{Dirichlet}) \quad (28b)$$

2.3. Wave Finite Element method in time domain

Based on frequency response of the structure issued from the FWFE method, the time response of the structure can be obtained in a rather simple way. For example, if a structure is subjected to an excitation force \mathbf{f}_{exc} in time domain $[t_k]_{k=1\dots M}$, through a Discrete Fourier Transform(DFT), the spectrum of this excitation force $\hat{\mathbf{f}}_{\text{exc}}$ can be expressed in the frequency domain $[\omega_k]_{k=1\dots M}$.

$$\hat{\mathbf{f}}_{\text{exc}}(\omega_k) = \sum_{m=1}^M \mathbf{f}_{\text{exc}}(t_m) e^{-jt_m \omega_k} \quad (29)$$

This spectrum is then used in the FWFE approach to calculate the nodal displacement response $\hat{\mathbf{u}}(\omega_m)$ frequency by frequency. Subsequently, by applying an Inverse Discrete Fourier Transform(IDFT) to the frequency response, the time response can be acquired.

$$\mathbf{u}(t_k) = \frac{1}{M} \sum_{m=1}^M \hat{\mathbf{u}}(\omega_m) e^{-jt_k \omega_m} \quad (30)$$

It should be noted that M , the number of samples should be large enough to ensure the quality of the frequency and time response.

2.4. Piezoelectric finite element formulation for the coupling element

In the Diffusion Matrix Model(DMM) [6, 9] mentioned in subsection 2.1, it is crucial to describe correctly the dynamics of the coupling element with shunted piezoelectric patches, in order to investigate the influence of the shunted piezoelectric patches on the propagation of wave modes in the thin-walled beam. In this subsection, an appropriate finite element formulation is developed.

A finite element model of the coupled system consisting of a rectangular thin-walled beam and 4 identic piezoelectric patches with shunted circuit is then established, as displayed in Figure 3.

Figure 3

Detailed piezoelectric constitution law is given in Appendix A. This model contains two thin-walled waveguides with 3D linear brick finite elements and a coupling element with 3D linear brick piezoelectric finite elements. The piezoelectric element has 8 nodes and 4 degrees of freedom(DOF) per node. Each node has 3 structural DOF and 1 electrical DOF (electrical potential). All electrical potential DOF that are placed on electrode surfaces of the patches are reduced such that only one potential master DOF remains. All electrical potential DOF on the patch surfaces bonded to the beam are grounded. The whole structure has free mechanical boundary conditions. For the sake of simplicity, detailed deductions of strain energy, mass and stiffness matrices for the piezoelectric elements (without shunt circuit), which

can be found in reference [21], are not presented in this paper. The discretized electro-elastic system of equations can be written in the form shown in equation (31a) and equation (31b).

$$\mathbf{M}_{dd}\ddot{\mathbf{d}} + \mathbf{K}_{dd}\mathbf{d} + \mathbf{K}_{dv}\mathbf{V} = \mathbf{F} \quad (31a)$$

$$\mathbf{K}_{dv}^T\mathbf{d} + \mathbf{K}_{vv}\mathbf{V} = \mathcal{Q} \quad (31b)$$

where \mathbf{d} and \mathbf{V} represent the structural and electrical DOF respectively, and:

$$\begin{aligned} \mathbf{M}_{dd} &= \int_{V_s} \mathbf{N}_d^T \rho \mathbf{N}_d dV & \mathbf{K}_{dd} &= \int_{V_s} \mathbf{B}_d^T \mathbf{c}^E \mathbf{B}_d dV & \mathbf{K}_{dv} &= \int_{V_s} \mathbf{B}_d^T \mathbf{e}^T \mathbf{B}_v dV \\ \mathbf{K}_{vv} &= - \int_{V_s} \mathbf{B}_v^T \epsilon^s \mathbf{B}_v dV & \mathbf{F} &= \int_{S_f} \mathbf{N}_d^T f dS & \mathcal{Q} &= - \int_{S_q} \mathbf{N}_v^T q dS \end{aligned} \quad (32)$$

in which \mathbf{N}_d and \mathbf{N}_v are the shape functions, $\mathbf{B}_d = \mathcal{D}\mathbf{N}_d$ and $\mathbf{B}_v = \nabla\mathbf{N}_v$. \mathcal{D} is the linear differential operator matrix which relates the strains to the structural displacements U . In this case, the matrix \mathcal{D} is given in equation (33).

$$\mathcal{D} = \begin{pmatrix} \frac{\partial}{\partial x} & 0 & 0 \\ 0 & \frac{\partial}{\partial y} & 0 \\ 0 & 0 & \frac{\partial}{\partial z} \\ \frac{\partial}{\partial y} & \frac{\partial}{\partial x} & 0 \\ 0 & \frac{\partial}{\partial z} & \frac{\partial}{\partial y} \\ \frac{\partial}{\partial z} & 0 & \frac{\partial}{\partial x} \end{pmatrix} \quad (33)$$

After finite element assembly, the discretized coupled piezoelectric and structural field equations are finally given in terms of nodal displacements u and nodal electric potential φ . The connection between the 4 piezoelectric patches

and the $R - L$ shunt circuit is displayed in Figure 4. It should be mentioned that by choosing the polarities of the piezoelectric patches, different wave modes can be targeted and controlled.

Figure 4

Following the electrode definitions mentioned in reference [19], the electrical potential DOF in the piezoelectric patches are partitioned into three different groups:

- For nodes on the outer surfaces of the piezoelectric patches, their associated electrical DOF are called φ_p , and they have the same electrical potential;
- For nodes on the inner surfaces of the piezoelectric patches bonded to the beam, their associated electrical DOF are called φ_g , and they are grounded;
- For nodes inside the piezoelectric patches, their associated electrical DOF are called φ_i .

The equations of motion are subsequently written in the form shown in equation (34).

$$\begin{bmatrix} \mathbf{M}_{uu} & 0 & 0 & 0 \\ 0 & 0 & 0 & 0 \\ 0 & 0 & 0 & 0 \\ 0 & 0 & 0 & 0 \end{bmatrix} \begin{bmatrix} \ddot{u} \\ \ddot{\varphi}_i \\ \ddot{\varphi}_p \\ \ddot{\varphi}_g \end{bmatrix} + \begin{bmatrix} \mathbf{K}_{uu} & \mathbf{K}_{ui} & \mathbf{K}_{up} & \mathbf{K}_{ug} \\ \mathbf{K}_{ui}^T & \mathbf{K}_{ii} & \mathbf{K}_{ip} & \mathbf{K}_{ig} \\ \mathbf{K}_{up}^T & \mathbf{K}_{ip}^T & \mathbf{K}_{pp} & \mathbf{K}_{pg} \\ \mathbf{K}_{ug}^T & \mathbf{K}_{ig}^T & \mathbf{K}_{pg}^T & \mathbf{K}_{gg} \end{bmatrix} \begin{bmatrix} u \\ \varphi_i \\ \varphi_p \\ \varphi_g \end{bmatrix} = \begin{bmatrix} \mathbf{F} \\ Q_i \\ Q_p \\ Q_g \end{bmatrix} \quad (34)$$

As $\varphi_g = 0$, the fourth equation and fourth column in the mass and stiffness matrices can be eliminated. Internal potential DOF can be determined by exact static condensation from equation (34) since internal electric charges $Q_i = 0$:

$$\varphi_i = -\mathbf{K}_{ii}^{-1}\mathbf{K}_{ui}^T u - \mathbf{K}_{ii}^{-1}\mathbf{K}_{ip}\varphi_p \quad (35)$$

Since all the nodes on the potential electrode surfaces have identical potentials, an explicit transformation matrix \mathbf{T}_m can be used to define the master potential DOF φ_m , as shown in equation (36).

$$\varphi_p = \mathbf{T}_m \varphi_m \quad (36)$$

The use of equation (36) yields the fully coupled dynamics:

$$\begin{bmatrix} \mathbf{M}_{uu} & 0 \\ 0 & 0 \end{bmatrix} \begin{bmatrix} \ddot{u} \\ \ddot{\varphi}_m \end{bmatrix} + \begin{bmatrix} \mathbf{H}_{uu} & \mathbf{H}_{up} \\ \mathbf{H}_{up}^T & \mathbf{H}_{pp} \end{bmatrix} \begin{bmatrix} u \\ \varphi_m \end{bmatrix} = \begin{bmatrix} \mathbf{F} \\ \mathbf{Q}_m \end{bmatrix} \quad (37)$$

with

$$\mathbf{H}_{uu} = \mathbf{K}_{uu} - \mathbf{K}_{ui}\mathbf{K}_{ii}^{-1}\mathbf{K}_{ui}^T \quad (38a)$$

$$\mathbf{H}_{up} = (\mathbf{K}_{up} - \mathbf{K}_{ui}\mathbf{K}_{ii}^{-1}\mathbf{K}_{ip})\mathbf{T}_m \quad (38b)$$

$$\mathbf{H}_{pp} = \mathbf{T}_m^T(\mathbf{K}_{pp} - \mathbf{K}_{ip}^T\mathbf{K}_{ii}^{-1}\mathbf{K}_{ip})\mathbf{T}_m \quad (38c)$$

$$\mathbf{Q}_m = \mathbf{T}_m^T \mathbf{Q}_p \quad (38d)$$

After the definition of the master DOF, the R-L shunt circuit can be considered. The electrical impedance of the circuit under harmonic excitation can be written as:

$$Z_{sh} = R + j\omega L \quad (39)$$

The current I_{sh} in the shunt circuit can be expressed as equation (40)

$$I_{sh} = j\omega \mathbf{Q}_m = \frac{\varphi_m}{Z_{sh}} \quad (40)$$

By substituting equation (40) into equation (37), the electrical DOF can be condensed and the equation that governs the structural dynamics under harmonic excitation is shown in equation (41).

$$[\mathbf{H}_{uu} - \omega^2 \mathbf{M}_{uu} + \mathbf{H}_{up} \left(\frac{1}{j\omega Z_{sh}} - \mathbf{H}_{pp} \right)^{-1} \mathbf{H}_{up}^T] u = \mathbb{D}u = \mathbf{F} \quad (41)$$

equation (41) gives a full finite element description of the beam with two symmetric shunted piezoelectric patches as a coupling element for the DMM calculation. Matrix \mathbb{D} represents the dynamical stiffness matrix of the coupling element.

3. Numerical simulations of thin-walled beams with shunted piezoelectric patches

In this section, the DMM with shunted piezoelectric elements is firstly employed to calculate the reflection and transmission coefficients of the pumping wave mode and the X -axis extensional wave mode. A full finite element description that takes the mechanical-electrical coupling into account is given to the thin-walled beams. The influence of the shunted piezoelectric patches on the propagation of these wave modes is carefully investigated. Subsequently, the FWFE approach is applied for the evaluation of the dynamical behavior of the structure in frequency domain. Unlike the DMM approach which gives predictions for the beam structure with free boundary conditions, frequency response functions can be obtained for the thin-walled beam structure with forced boundary conditions. Waveguides are of finite length in this case. Thereafter, based on the frequency responses, the calculation of time responses of the structure under wave packet excitation is carried out.

An extraction procedure is proposed to calculate reflection coefficients of the X -axis extensional mode so as to verify the results issued from the DMM approach.

3.1. DMM approach applied for pumping wave and X -axis extensional wave

The structures to be studied here are thin-walled beams with 4 identical $R-L$ shunted piezoelectric patches. The finite element model of the coupling element is shown in Figure 5, with the definition of geometric parameters. Two different cases are studied: in Case A the piezoelectric patches are bonded in a longitudinal way (see Figure 5(a)), while in Case B, these patches are bonded in a transversal way (see Figure 5(b)). Definitions and numerical values of the geometric parameters are listed in Table 1. The parameter L_b represents the length of the thin-walled beam involved in the coupling element. The material of the beam is aluminium and considered as isotropic, with Young's modulus $E_b = 70 \text{ GPa}$ and Poisson's ratio $\nu_b = 0.34$, and density $\rho_b = 2700 \text{ kg/m}^3$. The piezoelectric patches are fabricated by Saint-Gobain Quartz (type SG P189) and the corresponding material characteristics are listed in Appendix B. This type of piezoelectric patch works mainly in the 3-1 mode.

Figure 5

Table 1

At first, the thin-walled beam is regarded as a waveguide and the corresponding dispersion curves of the wave modes propagating in the structure

are extracted via the WFE approach, as shown in Figure 6. These curves describe the evolution of the wavenumber k in the frequency domain.

Figure 6

The wavelength(λ) of each mode can be calculated based on these results, as $\lambda = 2\pi/k$. The global mesh resolution is chosen to be $0.003 \times 0.005 \times 0.001 \text{ m}^3$, as the minimum wavelength of the concerned wave modes is about 0.04m in the concerned frequency band(from 0 to 12 kHz). In the finite element model of the waveguide there are 128 nodes/32 elements while in the coupling element there are 924 nodes/480 elements. The mode shapes of the wave modes propagating in the thin-walled beam are shown in Figure 7.

Figure 7

For the control of the symmetric pumping mode (Mode 6), the 2 horizontal piezoelectric patches should work in compression mode, whereas the 2 vertical piezoelectric patches should work in tension mode; for the control of the extensional mode, all the 4 patches should work in the same mode (tension or compression).

The DMM method is subsequently applied to the thin-walled beam in Case A for analyzing the symmetric pumping wave mode, and gives the reflection and transmission coefficients, as displayed in Figure 8(a), with $R = 10 \Omega$ and $L = 0.016 H$. The results for the X -axis extensional wave mode are shown in Figure 8(b).

Figure 8

The tuning frequency f_{tune} of the piezoelectric patches is about 9 kHz. Around this frequency, the impedance of the structure is greatly modified

by the shunted piezoelectric patches so that the wave propagation characteristics change significantly. The tuning frequency can be calculated according to equation (42):

$$f_{tune} = \frac{1}{2\pi\sqrt{4LC_{p3}^S}} \quad (42)$$

where $C_{p3}^S = (1 - k_{31}^2)C_{p3}^T$ is the capacitance of the piezoelectric patch measured at constant strain, and the 4 in front of L is due to the fact that the 4 piezoelectric patches are connected in parallel. If each piezoelectric patch has an independent shunt circuit, the 4 in front of L will disappear. The subscript 1 represents the X -axis direction while the subscript 3 denotes the Z -axis direction. k_{31} is the electromechanical coupling coefficient. C_{p3}^T is the capacitance of the piezoelectric patch measured at constant stress. It can be calculated in the following manner:

$$C_{p3}^T = \frac{\epsilon^T A_3}{L_3} \quad (43)$$

where A_3 is the area of the surface of the piezoelectric patch perpendicular to Z -axis, $L_3 = e_p$ is the thickness of the piezoelectric patch in Z -axis direction. Equally for the thin-walled beam in Case B, the reflection and transmission coefficients of the symmetric pumping mode and the extensional mode are shown in Figure 9.

Figure 9

It can be observed that the piezoelectric patches in Case A have a totally different effect on the symmetric pumping mode from the patches in Case B. This wave mode cuts on from about 5.6 kHz. In Case A, the piezoelectric patches are the most efficient around 8.5 kHz in the frequency band from 6

to 12 kHz, when the shunt circuit is open. In Case B, the shunted piezoelectric patches become less efficient from the cut-on frequency to about 7.5 kHz, and then the efficiency turns out to be better at higher frequencies. And in both cases, around the tuning frequency (about 9 kHz), the effect of the $R - L$ shunt circuit on the piezoelectric patches is rather evident. By simply varying the inductance L in the circuit, this tuning frequency can be displaced to desired frequency band. For the extensional wave in X -axis, in both cases, the shunted piezoelectric patches have similar influence on this wave mode. Around the tuning frequency, the patches in Case A results in a slightly stronger variation in the reflection and transmission coefficients, which indicates that the configuration in Case A is better for the control of the extensional wave in X -axis in this thin-walled beam.

3.2. Forced WFE applied for the control of symmetric pumping wave

For the calculation of the forced response of the thin-walled beam with shunted piezoelectric patches, the FWFE method mentioned in subsection 2.2 can be applied. The thin-walled beam to be studied is displayed in Figure 10.

Figure 10

In the formulation of FWFE, the lengths of the waveguides are no longer infinite and should be specified, as well as the boundary conditions. As shown in Figure 10, one extremity of the beam is excited by imposed displacement \mathbf{q}_{exc} , and the other extremity is free. The amplitude of the excitation displacement remains constant in the frequency domain. The imposed displacement is chosen to be one of the modal displacements so that only the mode with this modal displacement is excited in the thin-walled beam. The

first waveguide consists of N_1 identical unit cells while the second one consists of N_2 identical unit cells. The part of the beam covered with shunted piezoelectric patches is considered to be the coupling element. For the sake of simplicity, it is assumed that $N_1 = N_2 = N$. The two waveguides are identical as they belong to the same beam, thus $\Lambda_1^{\text{inc}} = \Lambda_2^{\text{ref}} = \Lambda$, and $\Lambda_1^{\text{ref}} = \Lambda_2^{\text{inc}} = \Lambda^{-1}$ (see equation (25)). The boundary conditions of the system can be written in the following manner:

$$\Phi_{\mathbf{q}1}^{\text{inc}} \mathbf{Q}_1^{\text{inc}(1)} + \Phi_{\mathbf{q}1}^{\text{ref}} \mathbf{Q}_1^{\text{ref}(1)} = \mathbf{q}_{\text{exc}} \quad (44a)$$

$$\Phi_{\mathbf{F}2}^{\text{inc}} \mathbf{Q}_2^{\text{inc}(N+1)} + \Phi_{\mathbf{F}2}^{\text{ref}} \mathbf{Q}_2^{\text{ref}(N+1)} = \mathbf{0} \quad (44b)$$

The boundary condition at the left extremity of Waveguide 1 is a Dirichlet boundary condition(equation (44a)), whereas the boundary condition at the right extremity of Waveguide 2 is a Neumann one(equation (44b)).

The continuity conditions of displacement and force between the waveguides and the coupling element form the coupling condition and can be expressed as:

$$\begin{bmatrix} \mathbf{q}_{\text{LC}} \\ \mathbf{F}_{\text{LC}} \end{bmatrix} = \begin{bmatrix} \mathbf{q}_{\text{R}1}^{(N+1)} \\ -\mathbf{F}_{\text{R}1}^{(N+1)} \end{bmatrix} \quad (45a)$$

$$\begin{bmatrix} \mathbf{q}_{\text{RC}} \\ \mathbf{F}_{\text{RC}} \end{bmatrix} = \begin{bmatrix} \mathbf{q}_{\text{L}2}^{(1)} \\ -\mathbf{F}_{\text{L}2}^{(1)} \end{bmatrix} \quad (45b)$$

where \mathbf{q}_{LC} and \mathbf{F}_{LC} stand for the nodal displacement and the nodal force at the left boundary of the coupling element, and \mathbf{q}_{RC} and \mathbf{F}_{RC} at the right boundary of the coupling element. By substituting these continuity conditions into the dynamics of the coupling element(see equation (41)), the boundary conditions at the right extremity of Waveguide 1 and those at the left extremity

of Waveguide 2 can be obtained, as shown in equation (46). \mathbb{D}^* denotes the dynamic stiffness matrix of the coupling element condensed on the DOFs located on the interfaces between the waveguides and the coupling element itself.

$$\mathbb{D}^* \begin{bmatrix} \mathbf{q}_{R1}^{(N+1)} \\ \mathbf{q}_{L2}^{(1)} \end{bmatrix} = - \begin{bmatrix} \mathbf{F}_{R1}^{(N+1)} \\ \mathbf{F}_{L2}^{(1)} \end{bmatrix} \quad (46)$$

Combined with the boundary conditions in equation (44a) and equation (44b) and the propagation relation(see equation (24)), an equation system which gives the wave amplitudes \mathbf{Q} in both waveguides under the excitation displacement \mathbf{q}_{exc} can be developed as follows:

$$\begin{bmatrix} \mathbf{\Phi}_{q1}^{\text{inc}} & \mathbf{\Phi}_{q1}^{\text{ref}} & \mathbf{0} & \mathbf{0} \\ (\mathbb{D}_{11}^* \mathbf{\Phi}_{q1}^{\text{inc}} + \mathbf{\Phi}_{F1}^{\text{inc}}) \Lambda^N & (\mathbb{D}_{11}^* \mathbf{\Phi}_{q1}^{\text{ref}} + \mathbf{\Phi}_{F1}^{\text{ref}}) \Lambda^{-N} & \mathbb{D}_{12}^* \mathbf{\Phi}_{q2}^{\text{inc}} & \mathbb{D}_{12}^* \mathbf{\Phi}_{q2}^{\text{ref}} \\ \mathbb{D}_{21}^* \mathbf{\Phi}_{q1}^{\text{inc}} \Lambda^N & \mathbb{D}_{21}^* \mathbf{\Phi}_{q1}^{\text{ref}} \Lambda^{-N} & \mathbb{D}_{22}^* \mathbf{\Phi}_{q2}^{\text{inc}} + \mathbf{\Phi}_{F2}^{\text{inc}} & \mathbb{D}_{22}^* \mathbf{\Phi}_{q2}^{\text{ref}} + \mathbf{\Phi}_{F2}^{\text{ref}} \\ \mathbf{0} & \mathbf{0} & \mathbf{\Phi}_{F2}^{\text{inc}} \Lambda^{-N} & \mathbf{\Phi}_{F2}^{\text{ref}} \Lambda^N \end{bmatrix} \begin{bmatrix} \mathbf{Q}_1^{\text{inc}(1)} \\ \mathbf{Q}_1^{\text{ref}(1)} \\ \mathbf{Q}_2^{\text{inc}(1)} \\ \mathbf{Q}_2^{\text{ref}(1)} \end{bmatrix} = \begin{bmatrix} \mathbf{q}_{\text{exc}} \\ \mathbf{0} \\ \mathbf{0} \\ \mathbf{0} \end{bmatrix} \quad (47)$$

The resolution of this equation system provides the wave amplitudes at the left boundary of the waveguides 1 and 2, and via equation (24), wave amplitudes at any node in the two waveguides can be obtained. As shown in Figure 10, the Z -axis component of the nodal displacement \mathbf{q}_{out} at the free extremity of the beam is used for the calculation of the frequency response function(FRF) of the thin-walled beam. As an example, the length of the waveguides is chosen to be 0.6 m , and the length of the unit cell in X -axis is 3 mm , thus $N = 200$. The pair of piezoelectric patches share the same shunt circuit with $R = 10 \ \Omega$ and $L = 0.016 \text{ H}$, in order to tune the wave modes around 9 kHz . The symmetric pumping mode is targeted, and its modal displacement at a fixed frequency(about 7 kHz) is taken as the im-

posed displacement excitation \mathbf{q}_{exc} . The FRF with shunt circuit and open circuit case are calculated numerically. Results for the beam in Case A are displayed in Figure 11.

Figure 11

As shown in Figure 11, the attenuation effect of the shunted piezoelectric patches around the tuning frequency (9 kHz), which is close to one of the eigenfrequencies of one of the symmetric pumping mode, is rather evident. In the same manner, another analysis is carried out for the thin-walled beam in case B (see Figure 5(b)). The comparison results of the FRF are shown in Figure 12.

Figure 12

In both Figure 11(a) and 12(a), it is clear that the pumping mode cuts on at about 5.6 kHz as the amplitude of the response becomes much larger from this frequency. These results reveal that FWFE can predict correctly the frequency response of the structure, and the efficiency of the FWFE formulation has already been tested and compared to classical FE method [10] or transfer matrix method [25]. It is an effective approach that can be employed to estimate the influence of the shunted piezoelectric patches on the symmetric pumping mode of the beam. It can also be concluded from Figure 11(b) and Figure 12(b) that the longitudinally bonded piezoelectric patches in Case A lead to a stronger attenuation effect than the transversally bonded patches in Case B.

It should also be noted that the FWFE formulation requires much less computational time compared to ANSYS, especially at high frequencies, where

very small element size is required to guarantee the computational precision with classical finite element method. Furthermore, ANSYS is not capable of analyzing shunt circuits with negative capacitance, but the FWFE method is able to deal with all kinds of shunt impedance.

3.3. Time response calculation and reflection coefficient verification

In Subsection 3.2, the frequency responses are calculated with an excitation displacement of constant amplitude in the frequency domain. In order to evaluate the time response, the approach mentioned in Subsection 2.3 is adopted. The reflection coefficients can be extracted from the time response and then be compared to those calculated with the DMM approach. This extraction technique can equally be applied in experiments to validate numerical results. Let's consider an aluminium beam with 4 identical longitudinally placed $R - L$ shunted piezoelectric patches in Case A. According to the dispersion curves shown in Figure 6, it can be noted that in the frequency band from 0 to 12 kHz, except the extensional mode in X -axis, the other modes are dispersive as their dispersion curves are not linear. As non-dispersive waves can maintain their wave form during the propagation, and their group velocity is almost constant, it will be much easier to track them in the structure. The group velocity of the extensional wave mode is shown in Figure 13. It is almost constant in the frequency band from 0 to 10 kHz.

Figure 13

Based on this group velocity, the length of the waveguides is chosen to be 2.4 meters which is large enough so that incident and reflected waves can be clearly distinguished. The same mesh resolution as that in the forced

response calculation in Subsection 3.2 is utilized. The structure is excited by uniformly distributed force in X -axis at one extremity. To minimize the effect of induced dispersion by the piezoelectric patches, narrow band signals are used, composed of 2.5 cycles modulated by a Hanning window with the central frequency f_0 equal to 7 kHz. The time wave form and the spectrum of this excitation force is displayed in Figure 14. The maximum amplitude is 0.1 N and the sampling frequency is 20 times greater than the central frequency in order to guarantee the signal quality of the wave packet.

Figure 14

This excitation force is amplified (by multiplying a constant gain G to the amplitude) and then applied to one extremity of the thin-walled beam as the input, and the X -axis component of the nodal displacement at the measure point is taken as the output, as shown in Figure 15. The measure point lies at 30 cm from the extremity with the imposed force.

Figure 15

Subsequently, the transfer function is calculated, as shown in Figure 16. The shunt circuit is tuned to about 9 kHz, with $R = 100 \Omega$ and $L = 0.016 H$, as one of the eigenfrequencies of this mode is close to 9 kHz. With the shunted piezoelectric patches, a damping effect is obtained for the X -axis extensional mode around the tuning frequency.

Figure 16

With this transfer function, the wave packet excitation is applied to the system in order to acquire the frequency response. Then the IDFT of this frequency response is carried out to calculate the time response of the structure,

as displayed in Figure 17. As those wave packets are apparently unconnected in this case, no wave packet decomposition techniques are needed.

Figure 17

In order to verify the reflection coefficients calculated via the DMM approach and provide an effective experimental evaluation technique for the reflection coefficient based on time response of the structure, the following extraction procedure is proposed:

1. The Hilbert Transform is applied to the time response of the structure, and its absolute value is representative of the envelope of the signal. The first peak represents the maximum amplitude of the incident wave, and the second peak for the reflected wave, as shown in Figure 18.

Figure 18

2. The imaginary part of the wavenumber k calculated with the WFE method is used to calculate the spatial damping. As the propagation of the mode can be characterized by an exponential law $A = A_0 e^{ikx}$, the spatial damping ratio $\gamma_x = - | \text{Im}(k) |$.
3. With the group velocity V_g of the wave mode, the damping ratio in time domain can be calculated as $\gamma_t = - | \text{Im}(k) V_g |$.
4. On the plot of the Hilbert Transform result, a damping curve can be drawn to take into account the damping effect caused by the distance between the measure point and the piezoelectric patches so as to evaluate the reflection coefficient correctly. This curve passes the first peak

of the Hilbert Transform result and follows the exponential decreasing law defined by $A = A_0 e^{\gamma t}$. \mathbf{A}_r denotes the amplitude of the reflected wave, and \mathbf{A}_i represents the amplitude of the incident wave with the attenuation effect taken into account, as shown in Figure 18. The reflection coefficient can be calculated as $\mathbf{R} = \mathbf{A}_r / \mathbf{A}_i$.

5. By varying the central frequency f_0 of the wave packet excitation, reflection coefficients at different frequencies can be acquired frequency by frequency in order to verify the reflection coefficients calculated with the DMM approach.

The reflection coefficients of the extensional wave mode tuned at 9 kHz are calculated via the DMM approach, and then compared to those obtained through the extraction procedure. It should be mentioned that this extraction procedure is a rather coarse evaluation tool for the reflection coefficients. If an error of $\pm 15\%$ is applied to each extracted reflection coefficient, then the envelope of the extracted reflection coefficients can be obtained. The results are shown in Figure 19.

Figure 19

For the frequency band below 6 kHz, it is difficult to evaluate correctly the reflection coefficient with the extraction procedure as the span of the wave packet in time domain becomes too large to distinguish incident and reflected waves, unless the length of the beam becomes larger. And for the frequency band around the tuning frequency, it is also difficult to evaluate precisely the reflection coefficient with the Hilbert Transform, as the added damping effect needs to be considered properly. On the whole, the results issued from the

DMM approach are verified by those through the extraction procedure, as the envelope covers most of the DMM results in the open circuit case. This procedure will be employed for the experimental validation of numerically calculated reflection coefficients.

4. Conclusions

Effective prediction tools for wave propagation characteristics and dynamic behavior of thin-walled structures equipped with shunted piezoelectric elements are provided. General formulations developed in this work can be applied for all kinds of slender smart structures. Generally, the main results can be summarized as follows:

- The finite element based WFE approach is developed, and the DMM formulation is extended to consider shunted piezoelectric elements. The wave modes propagating in the structure are correctly captured and the influence of the shunted piezoelectric patches on the control of the symmetric pumping mode and the X -axis extensional mode is investigated through the reflection and transmission coefficients of these wave modes.
- The forced responses of thin-walled structures excited in the symmetric pumping mode and the X -axis extensional mode are calculated via the FWFE formulation. The damping effect of the shunted piezoelectric patches can be well observed in the frequency responses.
- Time response of thin-walled structures excited with a wave packet form excitation is evaluated via an IDFT approach applied to the fre-

quency response. The X -axis extensional mode is targeted as it's non dispersive. By following an extraction procedure, reflection coefficients of this wave mode can be evaluated according to the time response of the structure so as to verify the reflection coefficients calculated through the DMM approach.

The numerical techniques presented in this work enable the evaluation of the performance of shunted piezoelectric patches on the control of wave propagation in thin-walled beams, and facilitate design modifications and systematic investigations of geometric and electric parameters of thin-walled beams with shunted piezoelectric patches. Intensive computations aiming at the design of the piezoelectric patch and the electronic shunt circuit on the patch such as optimizations of geometric and electric parameters can be carried out.

The experimental validation of the numerical results will be focused on in future work. And later the issue of wave propagation control in two-dimensional structures like stiffened panels [29, 30] using shunted piezoelectric patches will be investigated.

Acknowledgement

This work is supported by a collaborative research agreement (ANR NT09 617542) between Georgia Tech, FEMTO-ST Institute and Ecole Centrale de Lyon. We gratefully acknowledge Georgia Tech and the French ANR and CNRS for supporting such international collaborations.

Appendix A: Piezoelectric constitutive law

The three-dimensional piezoelectric constitutive law can be written as:

$$T = \mathbf{c}^E S - \mathbf{e}^T E \quad (48a)$$

$$D = \mathbf{e} S + \epsilon^S E \quad (48b)$$

where E denotes the electric field vector, T the mechanical stress vector, S the mechanical strain, and D the electric displacement vector; \mathbf{c}^E represents the material stiffness matrix, \mathbf{e} denotes the piezoelectric stress coupling matrix, and ϵ^S is the permittivity matrix under constant strain. Equation (48a) represents the indirect piezoelectric effect, whereas equation (48b) characterizes the direct piezoelectric effect.

Appendix B: material properties of the piezoelectric patch (type SG P189)

Mass density ρ : $\rho = 7650 \text{ kg/m}^3$.

Material stiffness matrix \mathbf{c}^E :

$$\mathbf{c}^E = 10^{10} \times \begin{bmatrix} 15.4 & 8.263 & 7.859 & 0 & 0 & 0 \\ 8.263 & 15.4 & 7.859 & 0 & 0 & 0 \\ 7.859 & 7.859 & 13.74 & 0 & 0 & 0 \\ 0 & 0 & 0 & 4.59 & 0 & 0 \\ 0 & 0 & 0 & 0 & 4.59 & 0 \\ 0 & 0 & 0 & 0 & 0 & 3.57 \end{bmatrix} \text{ Pa}$$

The piezoelectric stress coupling matrix \mathbf{e} :

$$\mathbf{e} = \begin{bmatrix} 0 & 0 & 0 & 0 & 12.88 & 0 \\ 0 & 0 & 0 & 12.88 & 0 & 0 \\ -6.187 & -6.187 & 12.80 & 0 & 0 & 0 \end{bmatrix} N/(V \cdot m)$$

The permittivity matrix under constant strain ϵ^S :

$$\epsilon^S = 10^{-8} \times \begin{bmatrix} 1.011 & 0 & 0 \\ 0 & 1.011 & 0 \\ 0 & 0 & 0.591 \end{bmatrix} C/(V \cdot m)$$

References

- [1] L. Gavric, Finite element computation of dispersion properties of thin-walled waveguides, *Journal of Sound and Vibration* 173 (1) (1994) 113–124.
- [2] L. Gavric, Computation of propagative waves in free rail using a finite element technique, *Journal of Sound and Vibration* 185 (3) (1995) 531–543.
- [3] A. S. Gendy, A. F. Saleeb, Vibration analysis of coupled extensional/flexural/torsional modes of curved beams with arbitrary thin-walled sections, *Journal of Sound and Vibration* 174 (2) (1994) 261–274.
- [4] M. Mitra, S. Gopalakrishnan, M. S. Bhat, A new super convergent thin walled composite beam element for analysis of box beam structures, *International Journal of Solids and Structures* 41 (5-6) (2004) 1491–1518.
- [5] L. Houillon, M. Ichchou, L. Jezequel, Wave motion in thin-walled structures, *Journal of Sound and Vibration* 281 (2005) 483–507.
- [6] J.-M. Mencik, M. N. Ichchou, Multi-mode propagation and diffusion in structures through finite elements, *European Journal of Mechanics - A/Solids* 24 (5) (2005) 877–898.
- [7] J.-M. Mencik, M. N. Ichchou, Wave finite elements in guided elastodynamics with internal fluid, *International Journal of Solids and Structures* 44 (2007) 2148–2167.

- [8] M. N. Ichchou, S. Akrouf, J.-M. Mencik, Guided waves group and energy velocities via finite elements, *Journal of Sound and Vibration* 305 (2007) 931–944.
- [9] M. N. Ichchou, J.-M. Mencik, W. Zhou, Wave finite elements for low and mid-frequency description of coupled structures with damage, *Computer methods in applied mechanics and engineering* 198 (15-16) (2009) 1311–1326.
- [10] W. Zhou, M. N. Ichchou, Wave scattering by local defect in structural waveguide through wave finite element method, *Structural Health Monitoring* 10 (4) (2011) 335–349.
- [11] W. Zhou, M. N. Ichchou, O. Bareille, Finite element techniques for calculations of wave modes in one-dimensional structural waveguides, *Structural Control and Health Monitoring* 18 (7) (2011) 737–751.
- [12] D. J. Mead, A general theory of harmonic wave propagation in linear periodic systems with multiple coupling, *Journal of Sound and Vibration* 27 (2) (1973) 235–260.
- [13] W. X. Zhong, F. Williams, On the direct solution of wave propagation for repetitive structures, *Journal of Sound and Vibration* 181 (3) (1995) 485–501.
- [14] J.-M. Mencik, M. N. Ichchou, A substructuring technique for finite element wave propagation in multi-layered systems, *Computer Methods in Applied Mechanics and Engineering* 197 (6-8) (2008) 505–523.

- [15] M. Collet, K. A. Cunefare, M. N. Ichchou, Wave motion optimization in periodically distributed shunted piezocomposite beam structures, *Journal of Intelligent Material Systems and Structures* 20 (7) (2009) 787–808.
- [16] N. W. Hagood, A. Flotow, Damping of structural vibrations with piezoelectric materials and passive electrical networks, *Journal of Sound and Vibration* 146 (1991) 243–268.
- [17] O. Thorp, M. Ruzzene, A. Baz, Attenuation and localization of wave propagation in rods with periodic shunted piezoelectric patches, *Journal of Smart Materials and Structures* 10 (5) (2001) 979–989.
- [18] C. H. Nguyen, S. J. Pietrzko, FE analysis of a PZT-actuated adaptive beam with vibration damping using a parallel R-L shunt circuit, *Finite elements in analysis and design* 42 (14-15) (2006) 1231–1239.
- [19] J. Becker, O. Fein, M. Maess, L. Gaul, Finite element-based analysis of shunted piezoelectric structures for vibration damping, *Computers and Structures* 84 (31-32) (2006) 2340–2350.
- [20] A. Spadoni, M. Ruzzene, K. A. Cunefare, Vibration and wave propagation control of plate with periodic arrays of shunted piezoelectric patches, *Journal of Intelligent Material Systems and Structures* 20 (8) (2009) 979–990.
- [21] F. Casadei, M. Ruzzene, L. Dozio, K. A. Cunefare, Broadband vibration control through periodic arrays of resonant shunts: experimental investigation on plates, *Journal of Smart Materials and Structures* 19 (1) (2010) 015002.

- [22] G. Wang, S. Chen, J. Wen, Low-frequency locally resonant band gaps induced by arrays of resonant shunts with antoniou's circuit: experimental investigation on beams, *Smart Materials and Structures* 20 (1) (2011) 015026.
- [23] T. L. Huang, M. N. Ichchou, O. A. Bareille, Multi-mode wave propagation in damaged stiffened panels, *Structural Control and Health Monitoring* (2011) doi: 10.1002/stc.451.
- [24] M. Collet, M. Ouisse, M. Ruzzene, M. N. Ichchou, Floquet-bloch decomposition for the computation of dispersion of two-dimensional periodic, damped mechanical systems, *International Journal of Solids and Structures* 48 (20) (2011) 2837–2848.
- [25] Y. Waki, B. R. Mace, M. Brennan, Numerical issues concerning the wave and finite element method for free and forced vibrations of waveguides, *Journal of Sound and Vibration* 327 (2009) 92–108.
- [26] J. Renno, B. Mace, On the forced response of waveguides using the wave and finite element method, *Journal of Sound and Vibration* 329 (2010) 5474–5488.
- [27] Y. Yong, Y. K. Lin, Propagation of decaying waves in periodic and piecewise periodic structures of finite length, *Journal of Sound and Vibration* 129 (2) (1989) 99–118.
- [28] J.-M. Mencik, M. N. Ichchou, L. Jézéquel, Propagation multimodale dans les systèmes périodiques couplés, *Revue Européenne de Mécanique Numérique* 15 (1-3) (2006) 293–306.

- [29] M. N. Ichchou, J. Berthaut, M. Collet, Multi-mode wave propagation in ribbed plates: Part I, wavenumber-space characteristics, *International Journal of Solids and Structures* 45 (5) (2008) 1179–1195.
- [30] M. N. Ichchou, J. Berthaut, M. Collet, Multi-mode wave propagation in ribbed plates: Part II, predictions and comparisons, *International Journal of Solids and Structures* 45 (5) (2008) 1196–1216.

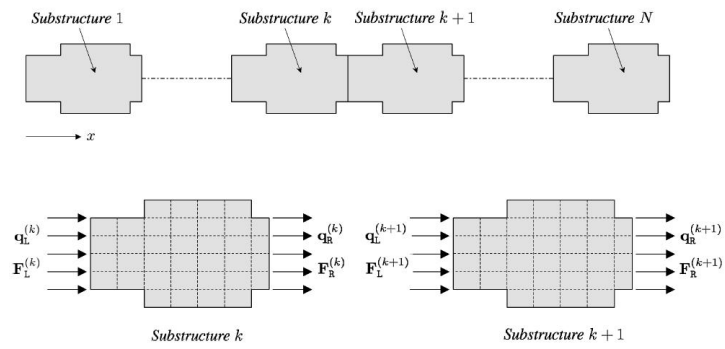


Figure 1: An illustration of a periodic waveguide [6].

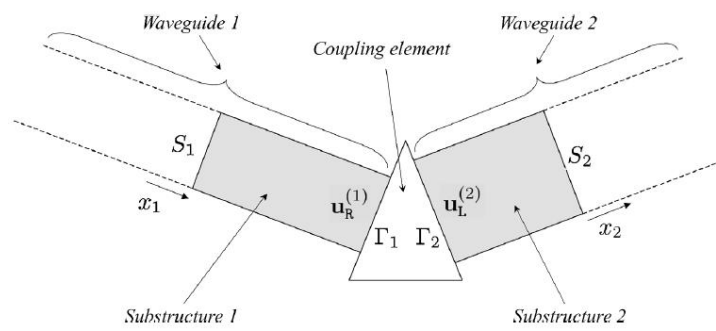


Figure 2: An illustration of the coupling between two different periodic waveguides [6].

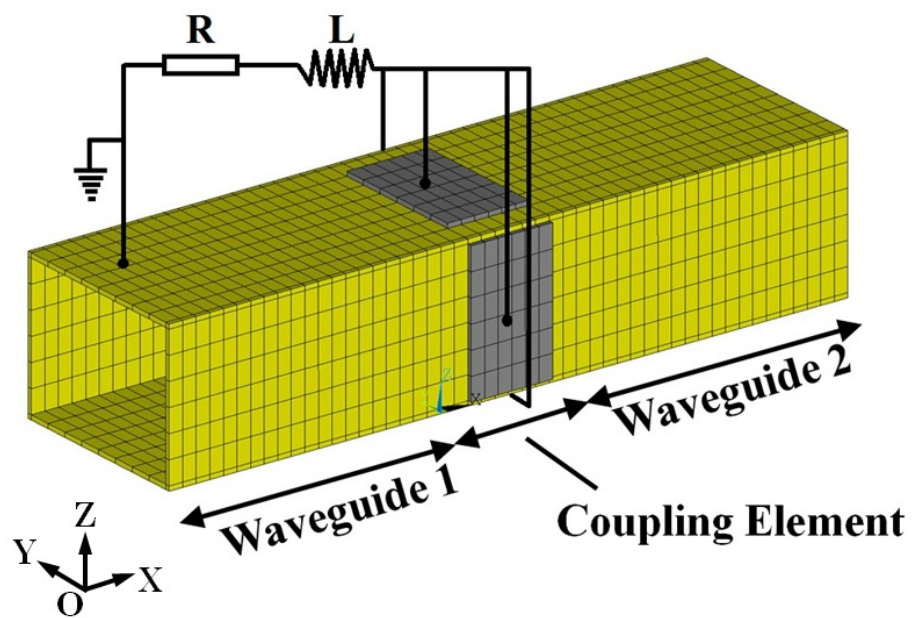


Figure 3: Finite element model of a thin-walled beam with symmetric shunted piezoelectric patches. The coupling element is the part of the beam with 4 identical piezoelectric patches.

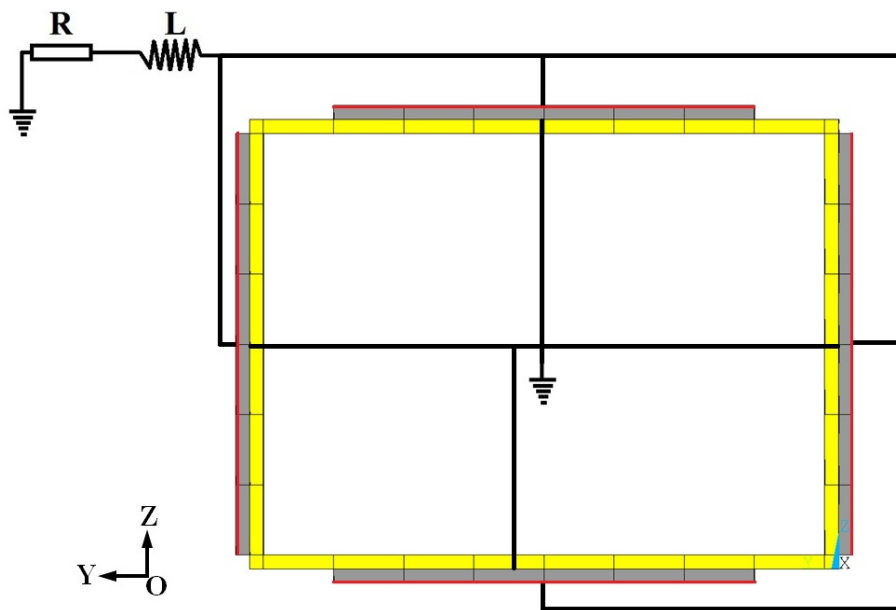
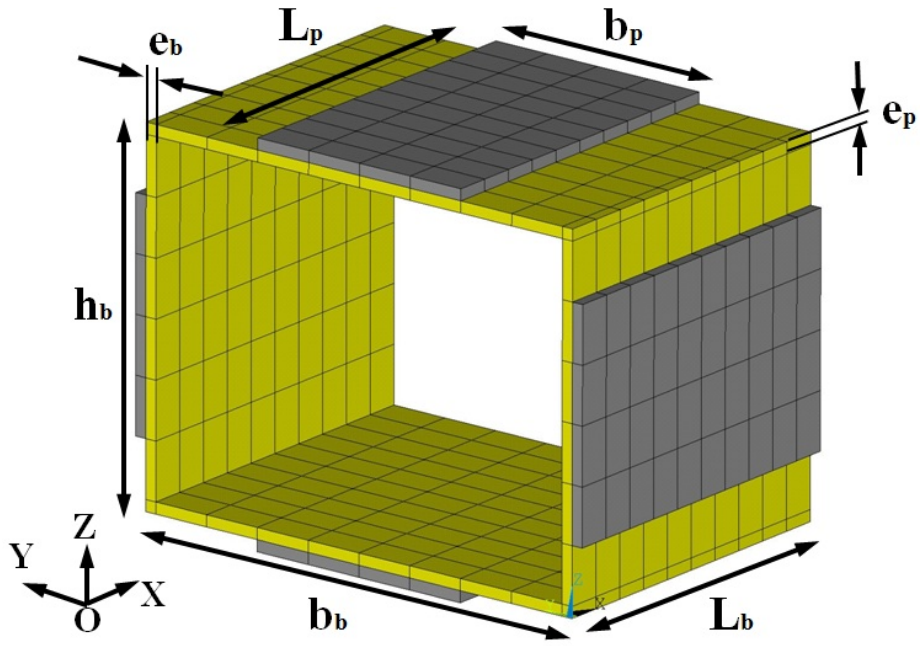
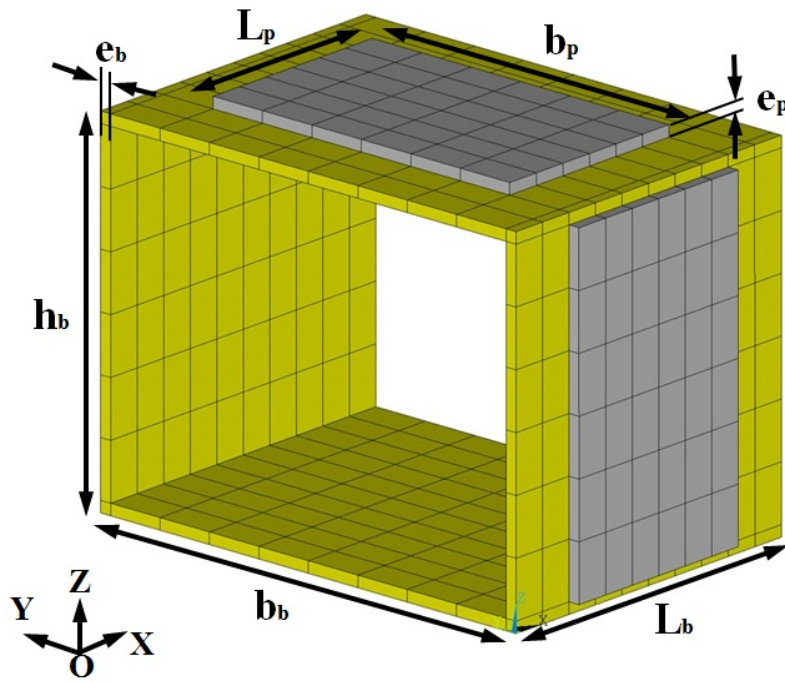


Figure 4: Configuration of the connection between the 4 piezoelectric patches and the $R-L$ shunt circuit.



(a)



(b)
45

Figure 5: Finite element model of the coupling element and definition of geometric parameters in (a)Case A(longitudinally bonded patches) (b)Case B(transversally bonded patches).

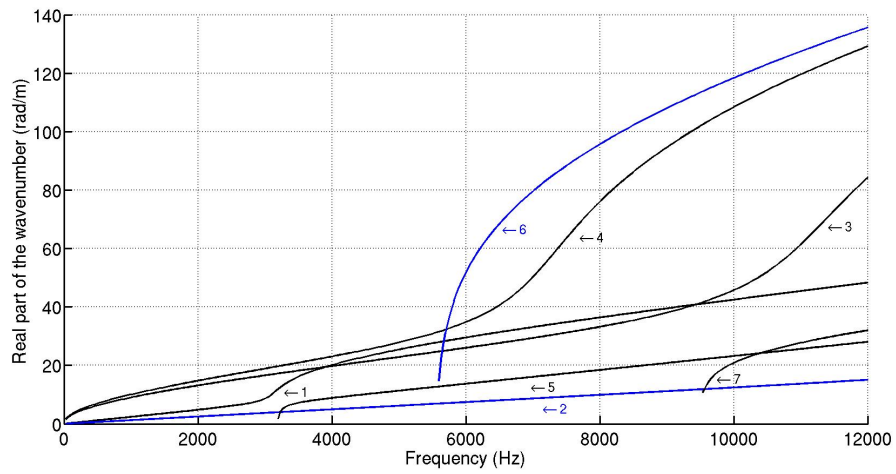


Figure 6: Dispersion curves of the wave modes propagating in the thin-walled beam in case A: (1)1st Torsional wave in X -axis (2)Extensional wave in X -axis (3)Flexural wave in Y -axis (4)Flexural wave in Z -axis. (5)2nd Torsional wave in X -axis. (6)Symmetric pumping mode. (7)Higher order cross-section mode. These wave modes are identified through their mode shapes (eigenvectors) issued from the WFE approach.

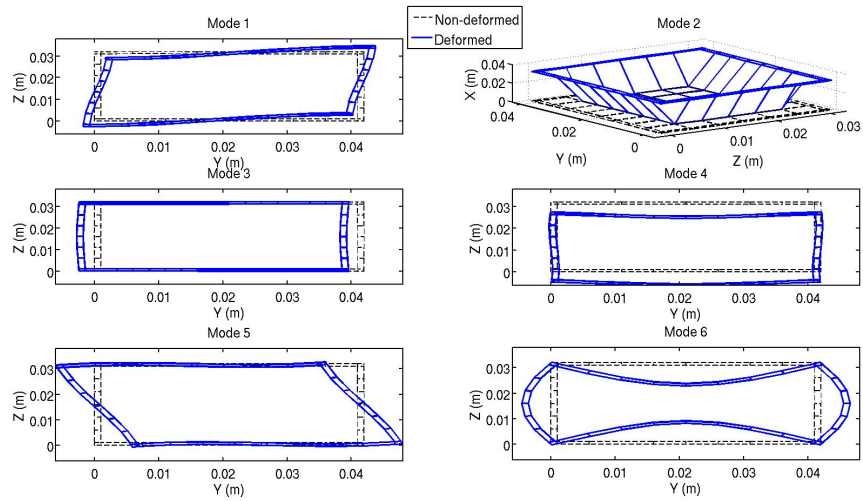
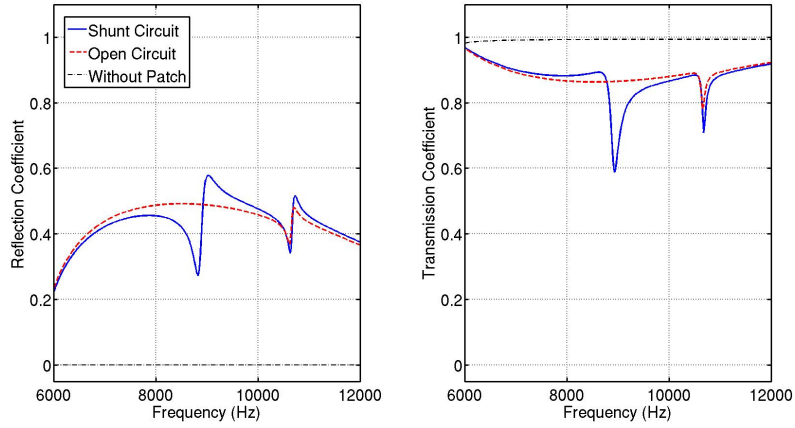
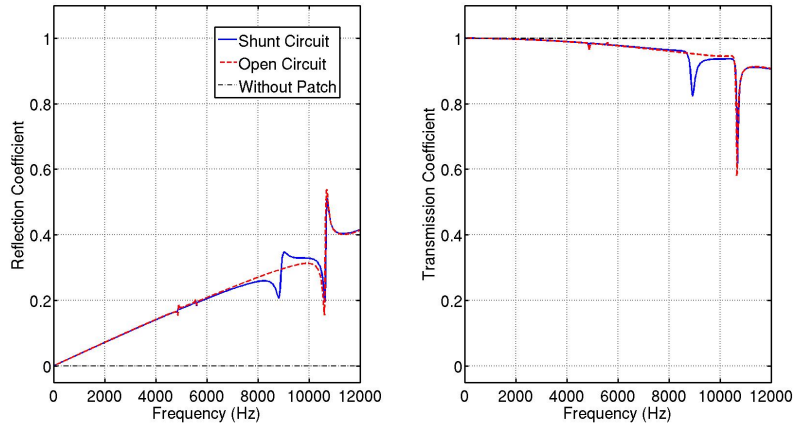


Figure 7: Mode shapes of the waves propagating in the thin-walled beam in case A: (1)1st Torsional wave in X -axis (2)Extensional wave in X -axis (3)Flexural wave in Y -axis (4)Flexural wave in Z -axis. (5)2nd Torsional wave in X -axis. (6)Symmetric pumping mode. (Solid line)Deformed mode shape. (Dashed line)Non-deformed section.

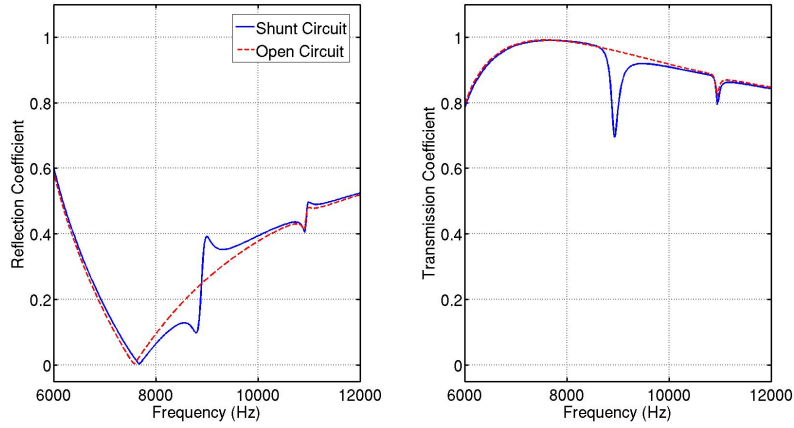


(a)

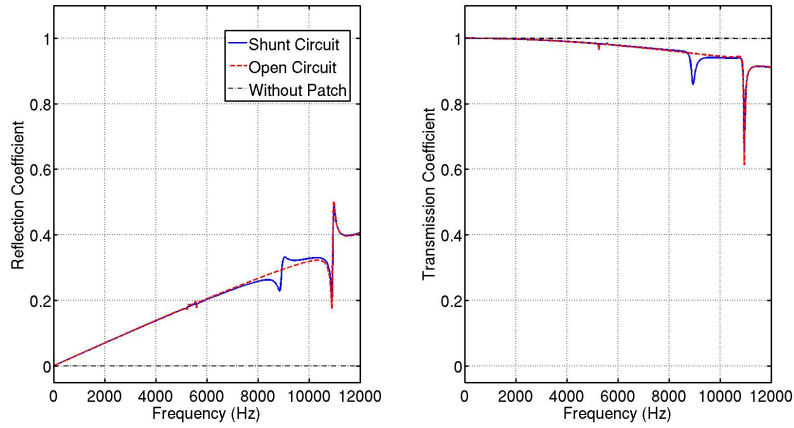


(b)

Figure 8: Reflection and transmission coefficients of wave modes in the thin-walled beam in Case A. (a)Symmetric pumping wave mode. (b) X -axis extensional wave mode. (Solid line)With R-L shunt circuit. (Dashed line)Shunt circuit open. (Point-dashed line)Beam without piezoelectric patches.



(a)



(b)

Figure 9: Reflection and transmission coefficients of wave modes in the thin-walled beam in Case B. (a)Symmetric pumping wave mode. (b)*X*-axis extensional wave mode. (Solid line)With R-L shunt circuit. (Dashed line)Shunt circuit open. (Point-dashed line)Beam without piezoelectric patches.

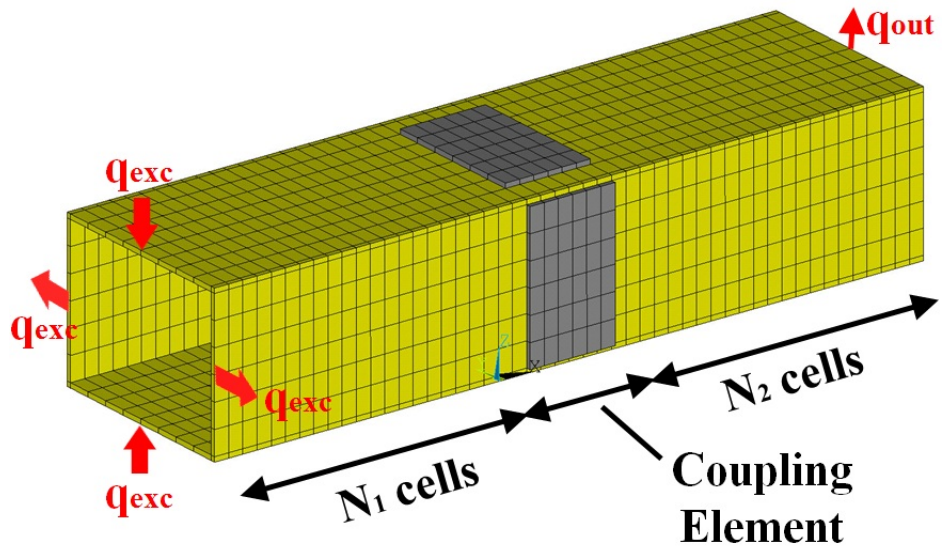
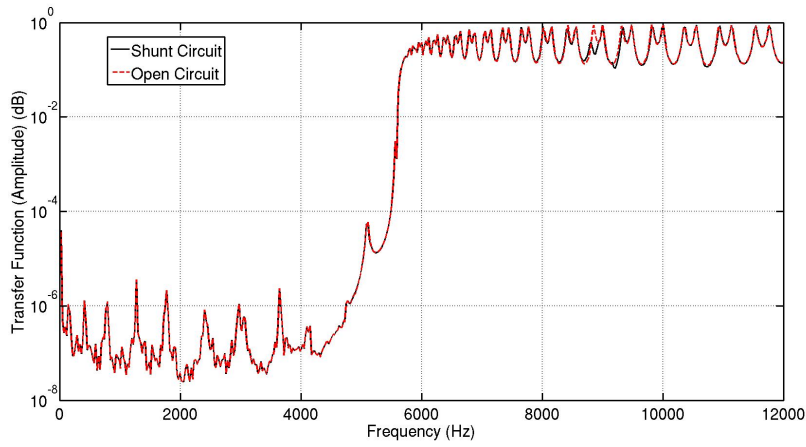
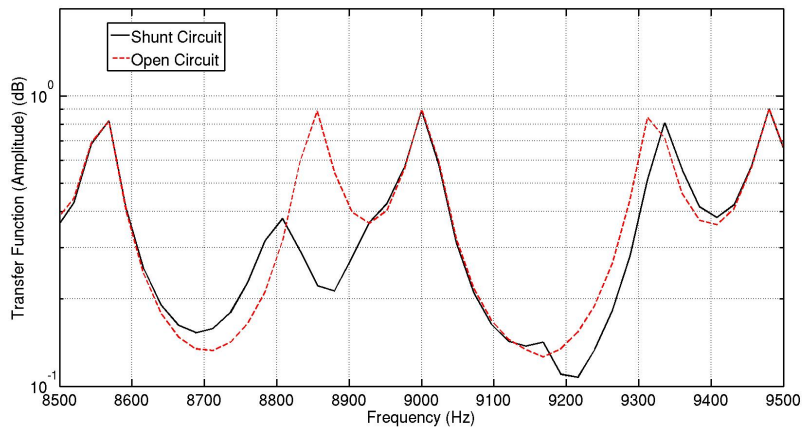


Figure 10: Finite element model for the calculation of the forced response of the thin-walled beam with 4 identical shunted piezoelectric patches.

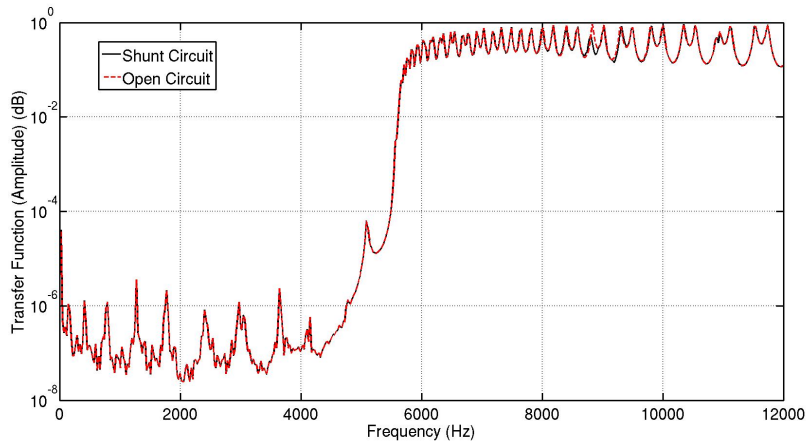


(a)

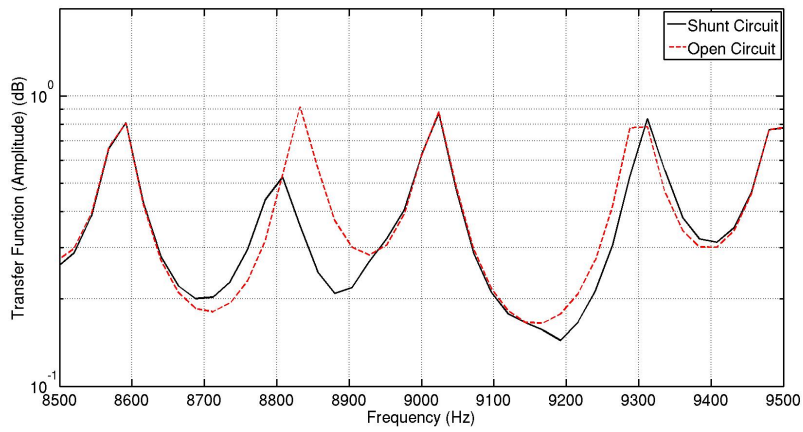


(b)

Figure 11: Comparison of the frequency responses in case A: (a) Frequency band from 6 to 12 kHz (b) Zoom around the tuning frequency (9 kHz). (Solid line)FWFE with shunted circuit. (Dashed line)FWFE without shunt circuit.



(a)



(b)

Figure 12: Comparison of the frequency responses in case B: (a) Frequency band from 6 to 12 kHz (b) Zoom around the tuning frequency (9 kHz). (Solid line)FWFE with shunted circuit. (Dashed line)FWFE without shunt circuit.

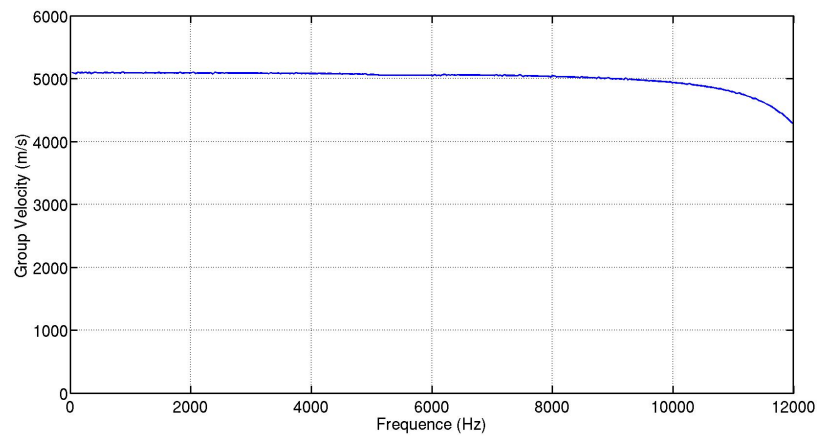
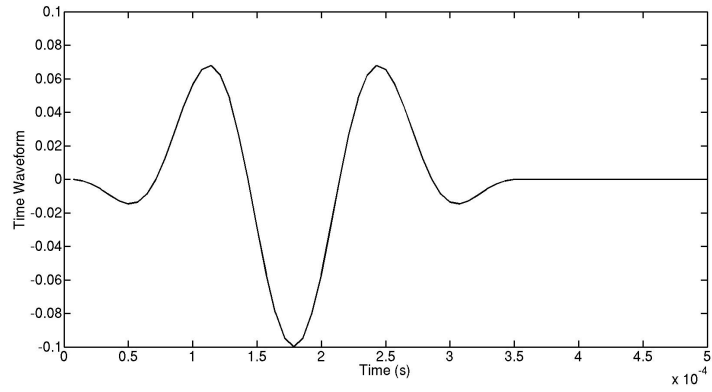
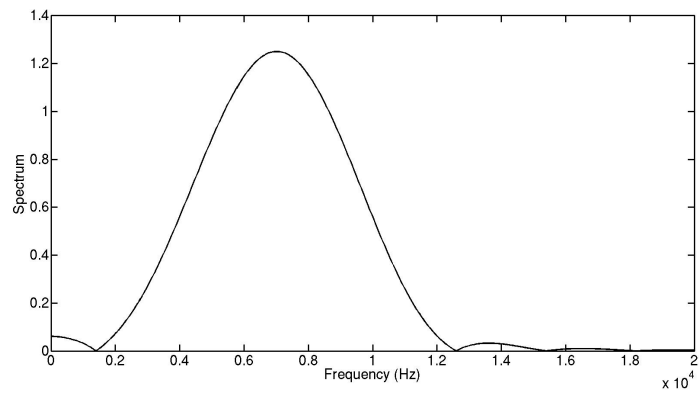


Figure 13: Group Velocity of the *X*-axis extensional wave.



(a)



(b)

Figure 14: The time wave form and the spectrum of the wave packet excitation. Central frequency $f_0 = 7 \text{ kHz}$. (a)Time wave form. (b)Spectrum.

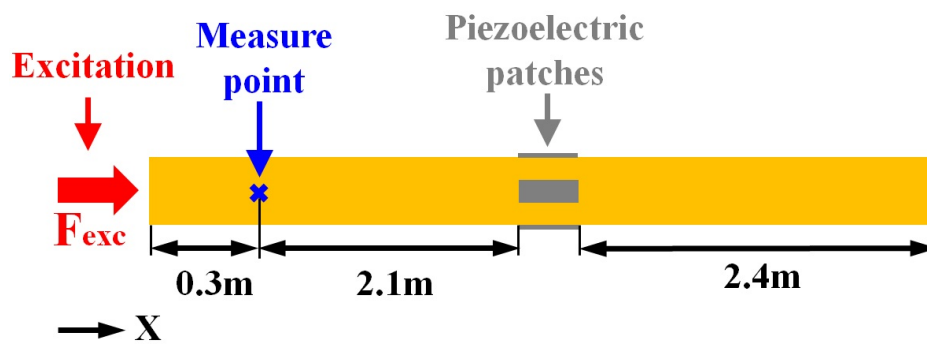


Figure 15: Configuration for the time response simulation of the X -axis extensional wave.

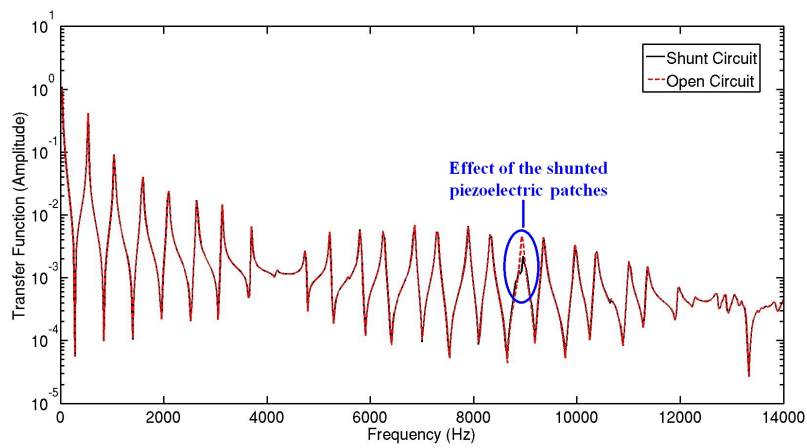


Figure 16: The forced response of the structure under white noise excitation (transfer function) tuned at 9 kHz. (Solid line) Piezoelectric patches with shunted circuit. (Dashed line) Shunt circuit open.

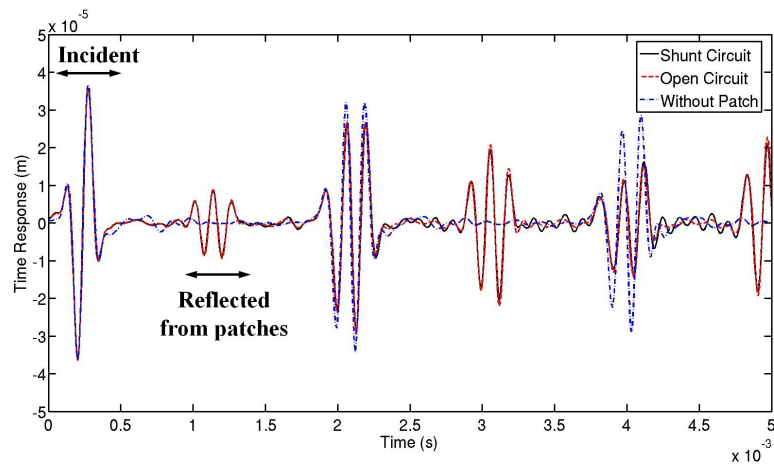


Figure 17: Time response of the structure under wave packet excitation. (Solid line) Piezoelectric patch with shunt circuit. (Dashed line) Piezoelectric patches with open shunt circuit. (Dash-dotted line) Beam without piezoelectric patches.

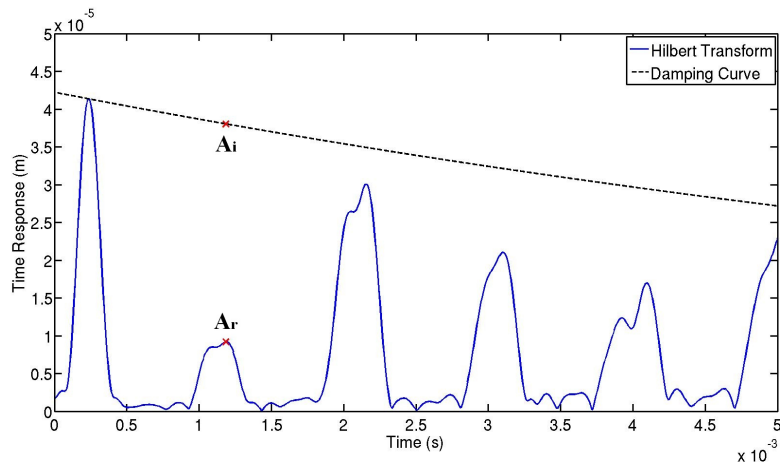


Figure 18: Hilbert Transform of the time response and the damping curve to extract the reflection coefficient of the X -axis extensional wave. (Solid line) Absolute value of the Hilbert Transform of the time response. (Dashed line) Damping curve based on spatial damping calculation.

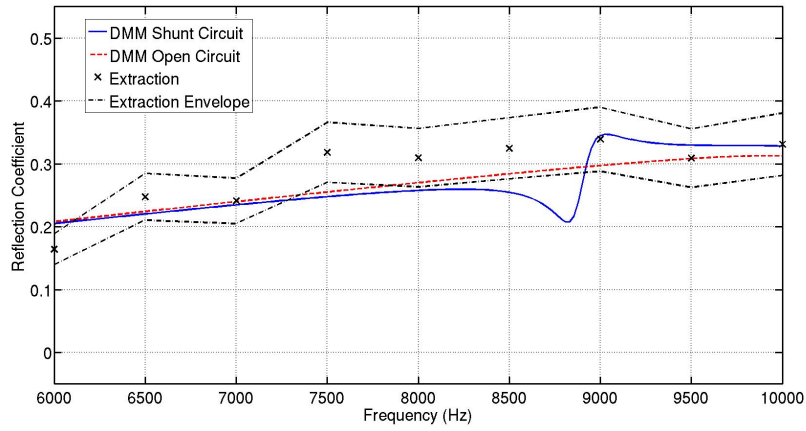


Figure 19: Comparison of reflection coefficients of the extensional wave in X -axis calculated through the DMM approach and the extraction procedure. (Solid line) Calculation with DMM, piezoelectric patch with shunt circuit. (Dashed line) Calculation with DMM, piezoelectric patch without shunt circuit. (\times markers) Calculation with extraction procedure. (Dash-dotted lines) Envelope of the extracted reflection coefficients.

Table 1: Numeric values of the geometric parameters in the coupling element shown in Figure 5. The units of all the parameters are in meter (m).

Case	L_b	L_p	b_b	b_p	h_b	e_b	e_p
A	0.03	0.03	0.042	0.02	0.032	0.001	0.001
B	0.03	0.02	0.042	0.03	0.032	0.001	0.001